applied sciences

MDPI

Article

A Split Ring Resonator-Based Metamaterial for Microwave Impedance Matching with Biological Tissue

Vincenza Portosi, Antonella Maria Loconsole and Francesco Prudenzano *

Department of Electrical and Information Engineering, Politecnico di Bari Via Orabona 4, 70125 Bari, Italy; vincenza.portosi@poliba.it (V.P.); antonellamaria.loconsole@poliba.it (A.M.L.)

* Correspondence: francesco.prudenzano@poliba.it

Received: 9 September 2020; Accepted: 24 September 2020; Published: 26 September 2020

Abstract: A metamaterial lens based on a split ring resonator (SRR) array has been designed and optimized to improve the focusing and the penetration depth in human biological tissue of a microwave beam irradiated by a substrate integrated waveguide (SIW) cavity backed patch antenna. The impedance matching of the antenna loaded with human tissue is strongly improved. The simulations have been performed by using CST Microwave Studio®. A prototype of the device has been fabricated with the printed board circuits (PCB) process and has been characterized using a Network Analyzer and an antenna measurement system in anechoic chamber. A novel microwave applicator for hyperthermia therapy of skin cancer could be developed. The performances of the proposed applicator have been evaluated in terms of measured S_{11} scattering parameter modulus and simulated power loss density. The obtained results indicate that an SRR-based metamaterial is a promising solution for external microwave applicators to employ in dermatology.

Keywords: split ring resonator (SRR); metamaterials; substrate integrated waveguide (SIW); planar antennas; microwave devices

1. Introduction

Microwave applicators have been proposed for applications in various areas, such as food cooking in domestic and industrial field, microwave-assisted extraction in environmental and chemical field [1,2], microwave-assisted synthesis in industrial material processing, bio-technology and chemical-pharmaceutics industry [3,4], drying, sterilization and disinfestation in agri-food [5,6] and microwave diathermy, hyperthermia cancer treatment and thermo-ablation therapy in medicine [7–13].

Microwave applicators for hyperthermia treatment in medical field are suitable antennas irradiating into the tissue to be treated in order to produce a sufficient heating of the entire tumor volume without damages of the surrounding healthy tissue. Microwave applicators can be divided into external and internal applicators depending on their peculiar use. External microwave applicators for superficial cancer, have been investigated and described in literature [7–13]. They typically consist of a single radiating element or of an antenna array placed in contact with the skin surface. A water bolus is usually placed between the applicator and the body in order to improve the matching of the antenna and at same time maintain the temperature of the skin at normal human body level. Among the various types of antennas studied for the external applicators there are waveguide and horn antennas [8], phased array antennas [9], and patch antennas [10–12]. Different shapes—rectangular, circular, and horseshoe—have been considered for the radiating slot of microstrip antennas for microwave hyperthermia treatment of cancer [13].

Patch antennas are considered very interesting radiating elements for the treatment of skin cancers because of their intrinsic advantages such as small size, low profile, light weight, high integration and low-cost fabrication. The design of the patch antenna and the choice of the operating frequency must take into account the size and depth of the tumoral mass. At low frequencies, a large penetration depth of the electromagnetic field can be obtained, but also the radiating system employed in order to produce an adequate localized heating becomes larger. Microstrip applicators, at 915 MHz, 433 MHz and 190 MHz, have been designed with low loss, high dielectric constant, substrate to treat tumors at 2 cm, 3 cm and 4 cm depth [7]. Among the principal drawbacks of patch antennas are the narrow bandwidth and low penetration depth capability. Several studies in the literature proved that metamaterial lens can improve the antenna directivity and reduce the beam width and side lobe ratio [14–17]. Left-handed metamaterial lenses have been numerically investigated in order to improve the focusing in superficial tumor [18,19]. Metamaterial zeroth-order mode applicators have been proposed in order to produce a more homogeneous specific absorption ratio (SAR) distribution, similar to that of an ideal plane wave, and larger penetration capability [20,21]. In particular, the metamaterials based on split ring resonator (SRR) are largely investigated since they offer several advantages, among which lightness, compact size and easy and low-cost fabrication.

Substrate integrated waveguide (SIW) technology allows to obtain an efficient and low-cost three-dimensional bounding of electromagnetic power via the planar printed board circuits (PCB) technology [22–28]. The metallic cavity improves the radiation performance of the patch antenna, increases the bandwidth and reduces the losses due to surface waves reduction [29].

In this paper, for the first time, to the best of our knowledge, a split ring resonator-based metamaterial is designed for the microwave therapy of cancer at the frequency $f = 10.7$ GHz. This frequency allows a good trade-off between the following needs: (a) good microwave absorption by biological tissue [30]; (b) small applicator size; and (c) localized/reduced ablation zone. Both (b) and (c) require the exploitation of high frequency. Generally, the SRR metamaterials are optimized for sensing/imaging applications at different operating frequencies. The design is focused (i) to improve the impedance matching of the antenna loaded with human tissue, thus avoiding the impedance mismatch and the formation of stationary waves which are deleterious for an efficient operation of the microwave applicator; (ii) to obtain a better focusing of the electromagnetic power into human tissue. This feasibility investigation constitutes a preliminary proof of concept for the development of a compact and low-cost microwave applicator for dermatology. The heating investigation is neglected in this paper, while the matching properties of metamaterial are experimentally demonstrated by employing a pre-prototype applicator which consists of a suitable SIW cavity-backed patch antenna with the optimized metamaterial lens based on SRR array. The antenna cavity has been designed by considering SIW technology. Higher gain, efficiency and directivity have been obtained by putting a SRR metamaterial over a patch antenna applicator. The impact of this research lies in the novelty of the proposed device and in its practical potential due to the possibility to refine a set of different SRR geometries. These can be optimized by considering the kind of organ, age and gender of the patients, for the same source and applicator. The obtained results pave the way towards the construction of an external microwave applicator for skin cancer thermal treatment.

2. Recall of Theory

In this section, the analytical model and physics of the split ring resonators is recalled since it has been employed in order to roughly obtain preliminary geometric parameters, before the actual design, which is numerically refined via CST Microwave Studio® as described in Section 3.

The metamaterial based on SRR exhibits an effective magnetic permeability described by the Lorentz model approximation [31,32]:

$$\mu_{r\mathrm{eff}}(\omega) = 1 - \frac{F\omega^2}{\omega^2 - {\omega_{0m}}^2 + j\gamma\omega} \quad (1)$$

where $\omega = 2\pi f$ is the angular frequency; ω_{0m} is the resonant frequency; F is the fractional of the unit cell occupied by interior ring; γ is the damping factor due to metal losses.

Starting from (1), a frequency range in which $\mathrm{Re}(\mu_{r\mathrm{eff}})$ is negative can be identified:

$$\omega_{0m} \; < \; \omega \; < \frac{\omega_{0m}}{\sqrt{1-F}} \; = \; \omega_{pm} \tag{2}$$

where ω_{pm} is the plasma magnetic frequency. Both ω_{pm} and ω_{0m} are finely tunable by optimizing the geometry of the unit cell.

When an electromagnetic wave propagates orthogonally to the SRR plane, the SRR behavior can be approximatively described by an equivalent LC circuit, where the inductance and the capacitance are related to the currents induced in the metal rings and to the capacitive phenomena between the split terminations (capacitive gap), respectively [32]. If the dimension of unit cell is very small with respect to wavelength λ, the metamaterial layer exhibits an effective capacitance and an effective inductance at the macroscopic/average level, according to the effective medium theory, which leads to the calculation of an effective permeability [31].

Considering a single broadside coupled SRR with square form rings in the xy plane, the effective magnetic permeability is described by (3) [14]:

$$\mu_{r\mathrm{eff}} = 1 - \frac{j\,\omega\,L_{\mathrm{eff}}\,S}{\Delta_x \Delta_y \left(R_{\mathrm{eff}} \; - \; \frac{j}{\omega\,C_{\mathrm{eff}}} \; + j\,\omega \; L_{\mathrm{eff}}\right)} \tag{3}$$

$$S = l_x l_y \tag{4}$$

where Δ_x and Δ_y are the dimensions of the SRR unit cell in xy plane; l_x and l_y are the lengths of the metallic ring in the x and y directions, respectively; R_{eff}, C_{eff} and L_{eff} are the effective resistance, effective capacitance and effective inductance of the metamaterial, respectively. The effective capacitance is approximatively obtained from the formula for the capacitance per unit length of a strip line [33].

$$C_{\mathrm{eff}} = \frac{\varepsilon_r\,\varepsilon_0\,l}{4}\,\frac{K(k)}{K'(k)} \tag{5}$$

$$k = \tan h \frac{\pi\,w}{2\,t} \tag{6}$$

$$l \; = \; 2\left(l_x + l_y - s\right) \tag{7}$$

where $K(k)$ and $K'(k)$ are elliptic integrals [34], w, s are the width and the split gap of the SRR; t is the distance between the two SRR in the z direction. The effective inductance is [33]:

$$L_{\mathrm{eff}} = \frac{\mu_0\,S}{t} \tag{8}$$

The effective resistance R_{eff} includes the radiation resistance and the loss resistance [33]. In other words, the control of the effective magnetic permeability, by varying both the inductive and capacitive properties of metamaterial, via a proper SRR optimization, is the basic physics principle of the electromagnetic field focusing. A planar metamaterial lens based on SRR, formed by an array of the unit cell in the rings plane, exhibits an anisotropic negative permeability; if the wave propagates in the z direction, the permeability tensor is [14]:

$$\mu = \mu_0 \begin{pmatrix} 1 & 0 & 0 \\ 0 & 1 & 0 \\ 0 & 0 & \mu_{r\mathrm{eff}} \end{pmatrix} \tag{9}$$

When the antenna radiation frequency is within the range for which the permeability element $\mu_{reff}(\omega) < 0$, the x-axis wave vector component is imaginary $k_x = \omega\sqrt{\varepsilon_y \mu_z}$, and therefore the component of the electromagnetic field parallel to SRRs plane is evanescent and the sideward radiation forbidden. Consequently, the main lobe of antenna radiation pattern will be improved while the side lobe is attenuated, and there is an overall improvement in terms of directivity and gain [15].

The metamaterial lens placed on the antenna, in addition to the electromagnetic field focusing properties, allowing the gain increasement, can be used as impedance matching layer. When the radiated electromagnetic waves propagate through media with different permittivity and permeability values an impedance mismatch occurs. The scheme of the normal wave propagation through the two layers sandwiched between two semi-infinite media is illustrated in Figure 1, where the SRR metamaterial layer is placed at distance t_2 from the biological layer to be matched.

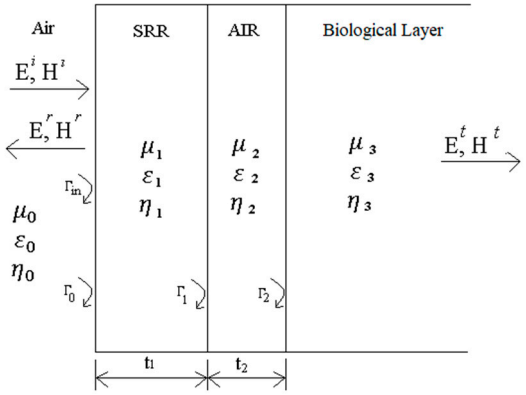

Figure 1. Scheme of the normal wave propagation through the two layers sandwiched between two semi-infinite media. The split ring resonator (SRR) metamaterial layer is placed to distance t_2 from the medium to be matched.

The metamaterial lens, if properly designed, can minimize the mismatch and maximize the energy transmission. With reference to Figure 1, the general form of wave matrices is given by (10).

$$\begin{bmatrix} E^i \\ E^r \end{bmatrix} = \prod_{n=1}^{3} \frac{1}{T_n} \begin{pmatrix} e^{i\gamma_n t_n} & \Gamma_{n-1} e^{-i\gamma_n t_n} \\ \Gamma_{n-1} e^{i\gamma_n t_n} & e^{-i\gamma_n t_n} \end{pmatrix} \begin{bmatrix} E^t \\ 0 \end{bmatrix} = \begin{pmatrix} a_{11} & a_{12} \\ a_{21} & a_{22} \end{pmatrix} \begin{bmatrix} E^t \\ 0 \end{bmatrix} \tag{10}$$

$$\Gamma_{in} = \frac{E^r}{E^i} = \frac{a_{21}}{a_{11}} \tag{11}$$

where T_n, γ_n and t_n are the transmission coefficient, propagation constant and thickness of the layer n, and Γ_{n-1} is the reflection coefficient at the $(n-1)-n$ layers interface. The total reflection coefficient of the multiple layers Γ_{in}, given by (11), is zero for a 'perfect' impedance match. By considering (11), the total reflection coefficient is a function of frequency and can be minimized by appropriately planning the effective magnetic permeability of the metamaterial and by adjusting the distance from the medium to be matched.

3. Design

The considered microwave applicator, depicted in Figure 2, is an SIW cavity-backed patch antenna, designed and optimized for Ku-Band applications (10.7–12.7 GHz). It consists of a stack structure: a microstrip patch antenna coupled with a circular resonant cavity based on SIW technology. The substrate Rogers Duroid 5880 with low dielectric constant $\varepsilon_r = 2.2$ and low losses tan $\delta = 0.0009$ has been considered for both layers. This antenna combines the attractive features of both SIW cavity-backed and patch antennas with truncated corners. The design has been performed by varying the size of the cavity, the hole diameters, the hole pitch, and the patch geometry. All the details

pertaining to designs of this kind of antenna are reported in [22]; they are not reported for shortness. The two cuts on the sides of the rectangular patch were designed to provide a wider frequency band and a frequency downshift. This allows a more compact size. The metallized cavity further broadens the bandwidth and improves the gain of the antenna; furthermore, the SIW technology offers the typical advantages of the standard PCB processes, such as easiness of fabrication, low cost, compact size and high integration with the planar circuits. Figure 3 shows the layout of an SIW cavity-backed patch antenna, the geometric parameters of which are listed in Table 1.

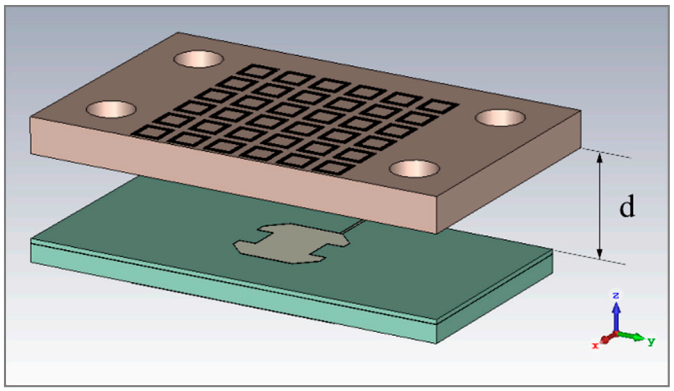

Figure 2. Layout 3D view of the microwave applicator with the split ring resonator-based metamaterial superstrate placed on the substrate integrated waveguide (SIW) cavity-backed patch antenna at a distance *d*.

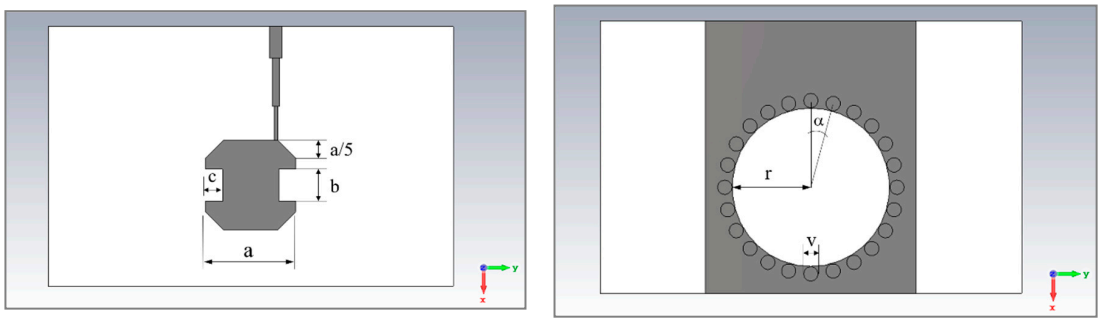

(**a**) (**b**)

Figure 3. Layout of SIW cavity-backed patch antenna. (**a**) Top view of the patch antenna and (**b**) top view of the SIW circular resonant cavity.

Table 1. List of the geometric parameters of the SIW cavity-backed patch antenna.

Parameter	Dimension	Description
a	8.00 mm	Length of the patch
b	2.86 mm	Length of the lateral cuts
c	1.50 mm	Width of the lateral cuts
r	6.72 mm	Radius of the SIW cavity
v	1.24 mm	Diameter of the vias
α	15°	Angular distance between the consecutive vias

The metamaterial theory reported in Section 2 has been applied to roughly identify the geometric parameters of the metamaterial operating at the Ku-Band applications. The analytical model for simple split ring resonators has been employed in order to obtain simple and preliminary line guides for the actual design, which is numerically performed via CST Microwave Studio®. The employed dielectric substrate is Rogers RO4350B with dielectric constant $\varepsilon_r = 3.48$ and dissipation factor of tan $\delta = 0.004$.

The geometry of the SRR unit cell has been suitably modified and scaled with respect to the literature [14] in order to operate at the resonance frequency of the SIW microwave applicator. Moreover, with respect to [14], the unit cell of the proposed SRR presents a further double ring with splits placed on the opposite side and operates at a different frequency. A complementary configuration, i.e., a couples of coplanar rings written symmetrically with respect to the common center, has been considered to obtain a resonance frequency close to that of a single ring with the same dimensions, but with a larger magnetic moment due to higher current density. Since they are written on both sides of a dielectric substrate, they are broadside coupled. The analytical model of a single (not complementary) broadside coupled SRR satisfactorily approximates the complementary configuration when the couple of rings are very close each other. The metamaterial considered in this paper consists of an array of complementary broadside coupled split square-rings. The lattice of this inhomogeneous structure is shorter than the guided wavelength of antenna radiation, so the composite behaves as an effective homogeneous medium.

The design and optimization of the metamaterial lens has been numerically performed via CST Microwave Studio®. After several simulations, in which the SRR geometry and cell size have been parametrically changed, the optimized geometric parameters are listed in Table 2. The optimized SRR metamaterial exhibits resonant frequency range overlapping the operating frequency range of the SIW cavity-backed patch antenna. Figure 4 shows the 3D view (a) and plan front view (b) of the unit cell of the SRR, respectively. The metamaterial lens used as superstrate of the SIW cavity-backed patch antenna is shown in Figure 5.

Table 2. List of the geometric parameters of the SRR Unit Cell of Figures 2, 4 and 5.

Parameter	Dimension (mm)	Description
Δx	3.20	Length of the unit cell in the x direction
Δy	3.20	Length of the unit cell in the y direction
l_{x1}	2.45	Length of the external SRR in the x direction
l_{y1}	2.45	Length of the external SRR in the y direction
l_{x2}	2.00	Length of the internal SRR in the x direction
l_{y2}	2.00	Length of the internal SRR in the y direction
s	0.11	Split gap of the SRR
w	0.11	Width of the SRR
g	0.11	Distance between the complementary SRRs in the xy plane
t	3.04	Distance between the broadside coupled SRRs in the z direction
d	6.90	Distance between the SIW antenna and the metamaterial lens
L_x	22.40	Length of the metamaterial lens in the x direction
L_y	36.00	Length of the metamaterial lens in the y direction

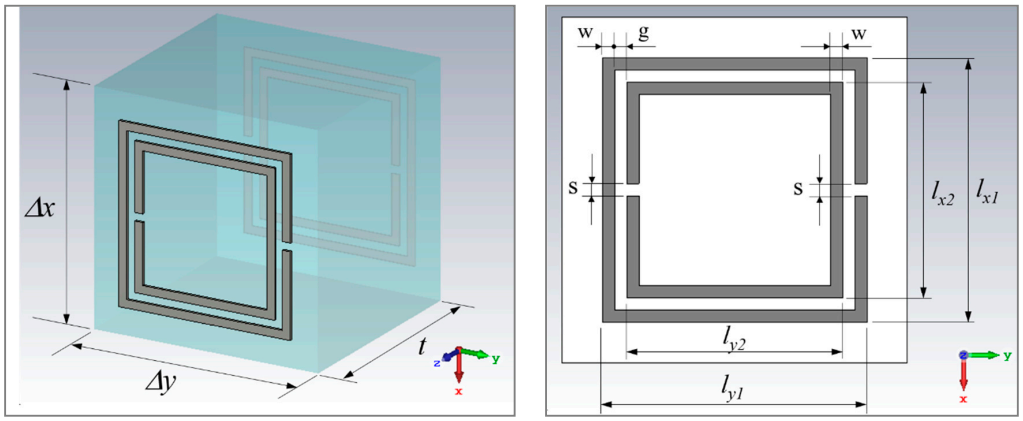

(**a**) (**b**)

Figure 4. 3D model of complementary broadside coupled SRR unit cell designed in CST Microwave Studio®. (**a**) 3D view and (**b**) top view.

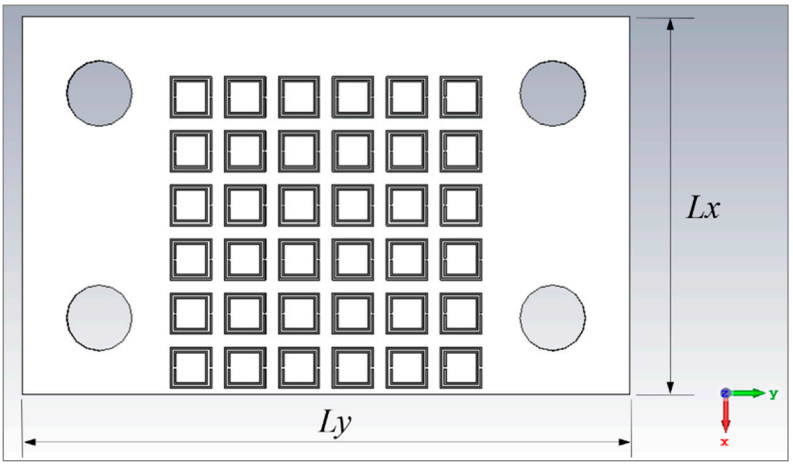

Figure 5. Layout of the SRR metamaterial placed as the patch antenna superstrate.

The S_{11} parameter of the microwave applicator placed at distance D from a model of human tissue is simulated to evaluate the lens metamaterial behavior as impedance matching layer. Figure 6 shows the sideview of the layout of SIW cavity-backed patch antenna covered by the metamaterial lens and at distance D from the biological tissue. The biological tissue considered in the simulation is a slab of skin-fat-muscle, whose electromagnetic parameters at the $f = 11$ GHz frequency are listed in Table 3 [35].

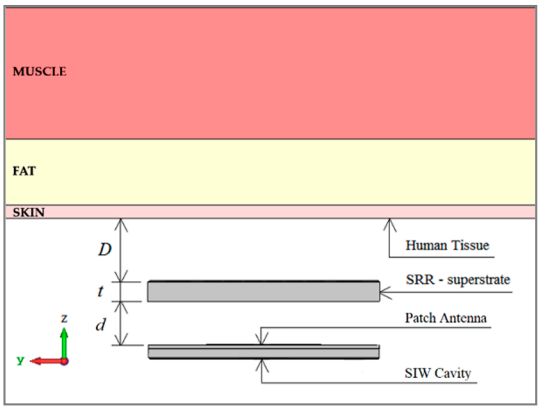

Figure 6. Sideview of SIW cavity-backed patch antenna with SRR superstrate placed at distance D from human tissue.

Table 3. Electromagnetic parameters human tissue at $f = 11$ GHz.

Biological Tissue	El. Conductivity (σ) (S·m^{-1})	Permittivity (ε)
Skin	9.1658	30.313
Fat	0.6567	4.5278
Muscle	12.083	41.419

The scattering parameter modulus $|S_{11}|$ of the SIW cavity-backed patch antenna with SRR superstrate has been simulated for different distances from the biological tissue, and the obtained results are compared in Figure 7a. It is apparent that the metamaterial placed at distance $D = 10$ mm allows the best impedance matching with the biological tissue. It is worthwhile noting that even if Figure 7a shows a narrow dip at $f = 10.9$ GHz, the overall operating bandwidth is typically defined at $|S_{11}| = -10$ dB level. Therefore, a very large frequency range of about 2 GHz can be exploited.

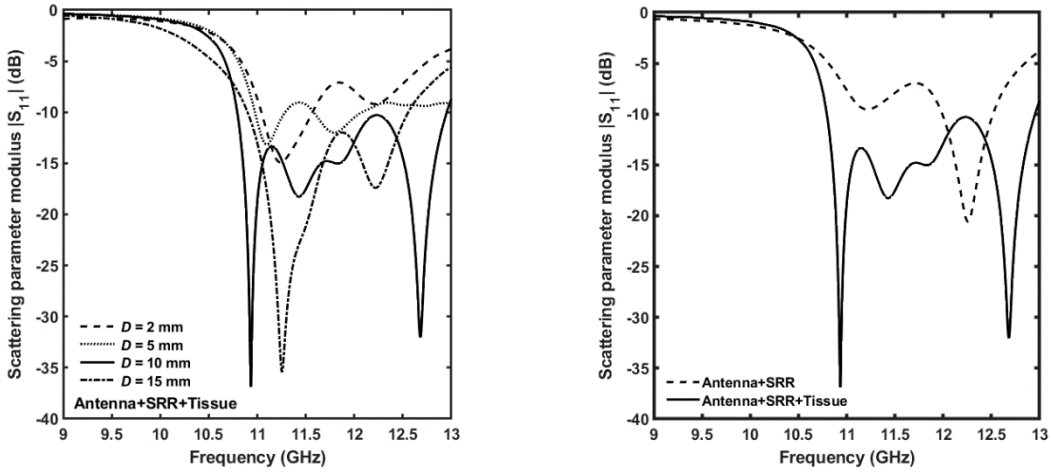

(**a**) (**b**)

Figure 7. Simulated scattering parameter modulus $|S_{11}|$ (**a**) of the SIW cavity-backed patch antenna with SRR superstrate placed at different distances from the biological tissue and (**b**) of the SIW cavity-backed patch antenna with SRR superstrate placed at distance $D = 10$ mm from the human tissue (continuous line) and of the SIW cavity-backed patch antenna with SRR superstrate without tissue (dashed line).

By considering the strong change of scattering parameter modulus $|S_{11}|$ with respect to the distance D, the following considerations can be inferred: (i) the distance D change induces the radiation impedance transformation of the applicator; (ii) the distance D could be optimized starting from the nominal value of $D = 10$ mm, by considering the particular biological tissue; (iii) suitable mechanical spacers could be finely controlled, e.g., by ad-hoc dielectric screws to optimize the microwave radiation. Figure 7b illustrates the simulated scattering parameter modulus $|S_{11}|$ of the SIW cavity-backed patch antenna with SRR superstrate placed at distance $D = 10$ mm from the human tissue (continuous line) and of the SIW cavity-backed patch antenna with SRR superstrate without tissue (dashed line). The reduction in the scattering parameter modulus $|S_{11}|$ can be observed over almost the entire frequency range, the metamaterial strongly improves the impedance matching.

The electric field distribution has been simulated in order to evaluate the ability of the proposed microwave applicator to focus the electromagnetic field into biological tissue. Simulated electric field 2D distribution in the yz plane at $f = 11$ GHz is reported in Figure 8.

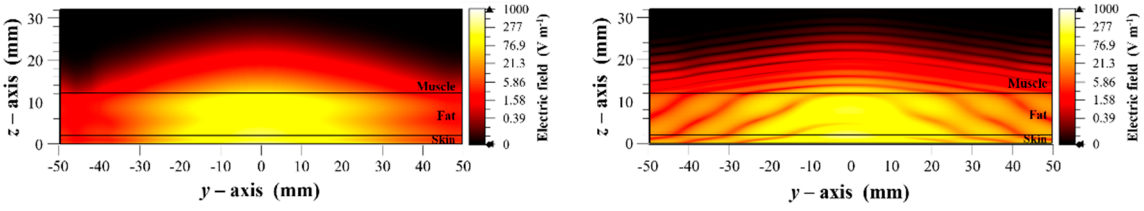

(**a**) (**b**)

Figure 8. Simulated electric field 2D distribution in the yz plane at the frequency $f = 11$ GHz; (**a**) SIW cavity-backed patch antenna with SRR superstrate placed at distance $D = 10$ mm from the human tissue; (**b**) SIW cavity-backed patch antenna placed at distance $D = 10$ mm from the human tissue without SRR superstrate.

The metamaterial lens produces a focusing improvement of the electromagnetic field into the skin model. In particular, in the case of SRR superstrate placed at distance $D = 10$ mm from the human tissue, the electric field modulus better penetrates along z-direction, in both the skin and fat layers, with respect to the case without SRR superstrate. Moreover, the region where the electric

field modulus is close to $|E| = 300$ Vm^{-1} is more homogeneous in the presence of SRR superstrate (Figure 8a). It is worth noting the nodal surfaces due to a stationary electromagnetic wave in absence of SRR metamaterial (Figure 8b).

4. Experimental

The antenna and metamaterial prototypes have been fabricated by employing the dielectric substrates Rogers Duroid 5880 with $\varepsilon_r = 2.2$ and $\tan\delta = 0.0009$ and Rogers RO4350B with $\varepsilon_r = 3.48$ and $\tan\delta = 0.004$, respectively, and by using a standard PCB process.

Top-views of the SIW cavity-backed antenna and the metamaterial lens are shown in Figure 9a, the four holes are fabricated to fixing with suitable screws the metamaterial lens to the SIW antenna and the nuts are screwed in order to the obtain the distance $d = 6.9$ mm, as shown in Figure 9b. The designed thickness of the metamaterial lens, $t = 3.04$ mm, is achieved by overlaying two layers of dielectric substrate each of thickness 1.52 mm. The scattering parameter S_{11} of the device has been measured with the Agilent Technologies N5224A Network Analyzer.

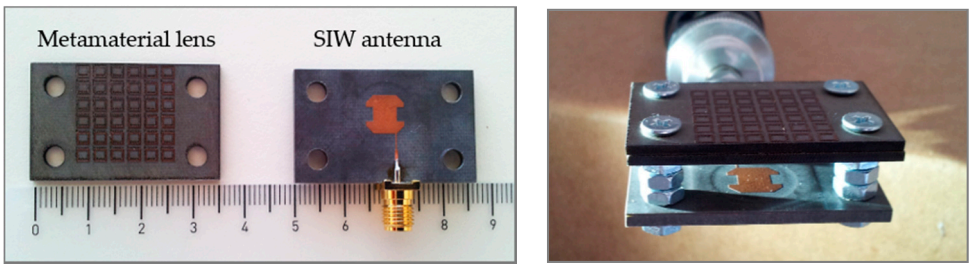

(**a**) (**b**)

Figure 9. (**a**) The metamaterial lens (at left) and SIW cavity-backed patch antenna (at right) prototypes. (**b**) SIW antenna and metamaterial superstrate assembled and connected to the Agilent Technologies N5224A Network Analyzer.

In Figure 10, the scattering parameter modulus $|S_{11}|$ of the SIW antenna versus the frequency with metamaterial lens is illustrated, the measurement is performed with the device that irradiates in air (dashed line) and in the biological tissue of a hand (continuous line) placed at a distance close to $D = 10$ mm from the SRR superstrate. The comparison highlights a good impedance matching of the microwave applicator loaded with the biological tissue in the frequency range 10.4–11.5 GHz. A scattering parameter modulus $|S_{11}|$ minimum of −42 dB at the 10.6 GHz frequency has been measured. Moreover, the measured results are in good agreement with simulated one of Figure 7b, although we can observe a shift of the resonance frequency of few hundred of MHz, in fact a scattering parameter modulus $|S_{11}|$ minimum of −36.9 dB at the 10.9 GHz frequency has been simulated. The second resonance frequency at $f = 12.7$ GHz of the simulated results is less pronounced respect to the experimental results around at $f = 12.3$ GHz. These differences may be due to manufacturing tolerances and the possible air film between the two layers of the dielectric that constitute the metamaterial lens.

Figure 11 shows the measured scattering parameter modulus $|S_{11}|$ of the SIW cavity-backed patch antenna, with (continuous line) and without (dashed line) the metamaterial superstrate that irradiates in the biological tissue. We can observe that the electromagnetic field of the antenna without the metamaterial lens is almost completely reflected from human tissue. We underline that the simulations of Figure 8 perfectly agree with the experimental results of Figures 10 and 11. In particular, in Figure 11, the measured scattering parameter modulus $|S_{11}|$ in the case of the antenna with SRR metamaterial and tissue (full curve) exhibits a strong dip close to the frequency $f = 10.7$ GHz. At the frequency $f = 11$ GHz, the impedance matching is good enough since the measured scattering parameter modulus is close to $|S_{11}| = -14$ dB. In fact, Figure 8a shows a homogeneous propagation/distribution of the simulated electromagnetic field. Moreover, Figure 11 shows that the measured scattering

parameter modulus in the case of antenna and tissue without SRR metamaterial (dashed curve) is close to $|S_{11}| = -4$ dB. This implies an impedance mismatch, the presence of the stationary wave and a not homogeneous distribution of the simulated electromagnetic field with nodal regions. It is in perfect agreement with the simulation in Figure 8b. In other words, the SRR metamaterial provides an impedance matching and a consequent suppression of the reflected wave.

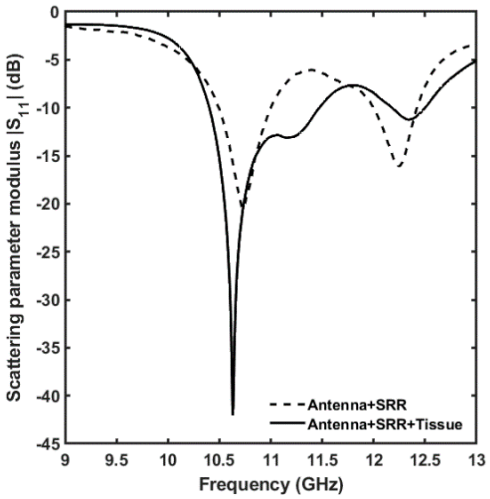

Figure 10. Measured scattering parameter modulus $|S_{11}|$ versus frequency of SIW cavity-backed patch antenna with metamaterial lens, that irradiates in biological tissue (continuous line) and in air (dashed line).

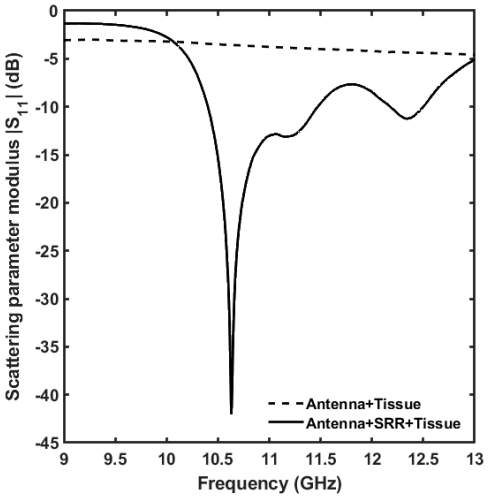

Figure 11. Measured scattering parameter modulus $|S_{11}|$ versus frequency of SIW cavity-backed patch antenna with (continuous line) and without (dashed line) the metamaterial superstrate that irradiates in the biological tissue.

The SIW antenna covered by the metamaterial layer has been characterized with the antenna measurement system in anechoic chamber, StarLab SATIMO, shown in Figure 12. The measured gain of the antenna with and without the metamaterial is illustrated in Figure 13, we can observe that SRR superstrate produces an improvement of the gain in the frequency range over $f = 11$ GHz with an increasement of 4 dB at $f = 12.2$ GHz.

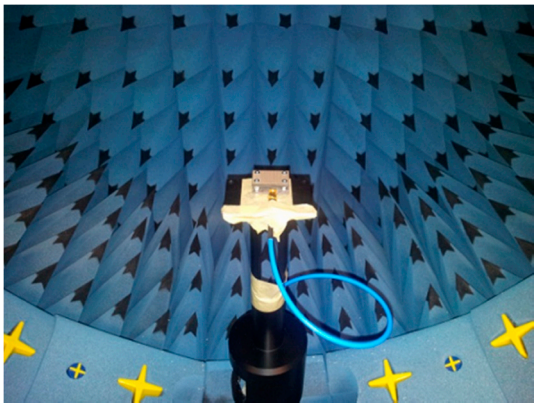

Figure 12. SIW cavity-backed patch antenna with metamaterial lens in the anechoic chamber StarLab SATIMO.

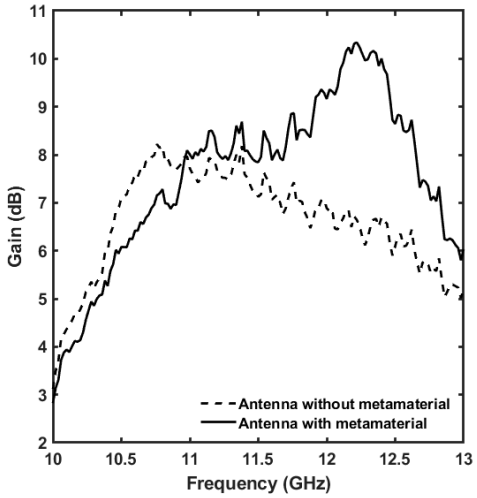

Figure 13. Measured gain versus frequency of SIW cavity-backed patch antenna with and without metamaterial.

Even if the aim of the paper is the optimization of the impedance matching with the biological tissue, we performed the simulation of the SIW cavity-backed patch antenna covered by the metamaterial and loaded with a biological tissue, i.e., a slab of skin-fat-muscle, whose electromagnetic parameters at the $f = 11$ GHz frequency are reported in Table 3, in order to compare the proposed device with the literature. A comparison with other microwave applicators is complex, due to the large variety of parameters characterizing the investigations reported in literature, among which the kind of antenna, frequency, kind of metamaterial, applied microwave power and obtained performances characterized in terms of Heating Zone Dimension (HZD), SAR zone, maximum temperature at focusing depth, etc.

For the proposed applicator, the peak SAR averaged over the mass $m = 1$ g and over the mass $m = 10$ g, the 50% SAR zone, the 42 °C HZD, for an input power $P = 1$ W at $f = 11$ GHz frequency are evaluated, in the case of the microwave applicator placed at distance $D = 10$ mm from the skin surface of the human tissue. Table 4 shows that the obtained results are interesting if compared with those from the literature. The reduced HZD zone and high SAR peak evidence the strong focusing obtained via the designed SRR metamaterial. This paves the way for promising novel applications.

Table 4. Comparison with other microwave applicators for cancer therapy.

Ref/ Year	Antenna/Frequency	Metamaterial	Biological Tissue	Results
[19] 2009	Line source extended infinitely/2.45 GHz	Flat left-handed metamaterial (LHM)	Superficial tumor	$T_{max} = 44.7$ °C at 0.71 cm below the skin surface 42 °C HZD of 1 cm × 1.2 cm Electromagnetic field source 43.44 Vcm^{-1}
[36] 2011	Dipole antenna/4.15 GHz	Flat left-handed metamaterial (LHM)	Breast tissue	$T_{max} = 46$ °C at 7.5 cm from the border of the LHM lens Input power $P = 8$ W
[18] 2012	Multiple Line source extended infinitely/2.45 GHz	Flat left-handed metamaterial (LHM)	Superficial tumor	42 °C HZD of 6.2 cm × 1.3 cm
[20] 2014	Zero-order resonator antenna/434 MHz	Zero-order resonator (ZOR) metamaterial	Superficial tumor	50% SAR zone of 6 cm × 24 cm
[37] 2015	Multiple microwave sources/6 GHz	Flat left-handed metamaterial (LHM)	Breast tissue	42 °C HZD of 4.76 cm × 1.14 cm × 0.92 cm, one LHM lens 42 °C HZD of 1.13 cm × 0.89 cm × 0.61 cm, two LHM lens 42 °C HZD of 0.87 cm × 0.87 cm × 0.61 cm, four LHM lens
[38] 2016	Microstrip antenna/2.45 GHz	Electromagnetic band gap (EBG)	Breast tissue	Peak $SAR_{1\,g} = 25$ mWg^{-1} Peak $SAR_{10\,g} = 4.54$ mWg^{-1} Input power $P = 1$ W
[39] 2017	Coaxial antenna/2.45 GHz	Left-handed metamaterial (LHM)	Superficial tumor	50% SAR zone of 1.81 cm × 0.32 cm
This work	SIW cavity backed patch antenna/Ku-band	Split ring resonator (SRR)	Superficial tumor	Peak $SAR_{1\,g} = 51.1$ mWg^{-1} Peak $SAR_{10\,g} = 14.2$ mWg^{-1} 50% SAR zone of 1.6 cm × 0.2 cm 42 °C HZD of 1.4 cm × 1.3 cm × 0.4 cm Input power $P = 1$ W at $f = 11$ GHz

5. Conclusions

A metamaterial lens based on SRR has been designed to be employed as a lens to be put on an SIW cavity-backed patch antenna in order to improve the impedance matching of the antenna when loaded with human tissue and to enhance the focusing of the electromagnetic field into the biological tissue to be treated. A prototype has been fabricated employing the standard, low cost PCB technology and has been characterized by using a Network Analyzer. The simulated scattering parameter modulus of the antenna loaded with the biological tissue with and without metamaterial lens is $|S_{11}| = -37$ dB and $|S_{11}| = -14$ dB at the $f = 11$ GHz frequency, respectively. The measured minimum of the scattering parameter modulus $|S_{11}| = -42$ dB has been measured at the $f = 10.6$ GHz frequency. The experimental results are in good agreement the simulations. The impedance matching improvement has been proved. The electromagnetic field distributions simulated have highlighted the focusing capability of the metamaterial lens. The antenna measurement in the anechoic chamber has confirmed that this kind of SRR lens can find actual application to focus the electromagnetic field of microwave applicators used in dermatology for the thermal therapy of skin cancer.

Author Contributions: Conceptualization, Investigation and Methodology, V.P., A.M.L., F.P.; Writing—Original Draft Preparation, V.P., F.P.; Review and Editing, V.P., A.M.L., F.P.; Supervision, F.P. All authors have read and agreed to the published version of the manuscript.

Funding: This research received no external funding.

Acknowledgments: This work has been partially supported within projects: POR FESRFSE 2014–2020 Innonetwork "Sinach-Integrated systems for mininvasive surgical navigation"—n. BLNGWP7; PON R&I 2014–2020 "New Satellites Generation components—NSG" n. ARS01_01215 NSG; MIUR "Agricolture Green & Digital—AGREED", PNR 2015–2020, n. ARS01_00254.

Conflicts of Interest: The authors declare no conflict of interest.

References

1. Delazar, A.; Nahar, L.; Hamedeyazdan, S.; Sarker, S. Microwave-Assisted Extraction in natural products isolation. In *Methods in Molecular Biology*; Sarker, S., Nahar, L., Eds.; Humana Press: Clifton, NJ, USA, 2012; Volume 864, pp. 89–115.
2. Veggi, P.C.; Martinez, J.; Meireles, M.A.A. Fundamentals of Microwave Extraction. In *Microwave-Assisted Extraction for Bioactive Compounds*; Chemat, F., Cravotto, G., Eds.; Food Engineering Series; Springer: Boston, MA, USA, 2012; pp. 15–52.
3. Safarik, I.; Horska, K.; Pospiskova, K.; Maderova, Z.; Safarikova, M. Microwave assisted synthesis of magnetically responsive composite materials. *IEEE Trans. Magn.* **2013**, *49*, 213–218. [CrossRef]
4. Ariffin, M.F.K.; Idris, A.; Ngadiman, N.H.A. Optimization of one-pot microwave-assisted ferrofluid nanoparticles synthesis using response surface methodology. *IEEE Trans. Magn.* **2018**, *54*, 1–6. [CrossRef]
5. Bozzetti, M.; Calò, G.; D'Orazio, A.; Petruzzelli, V.; Prudenzano, F.; Diaferia, N.; Bonaventura, C. Mode-stirred chamber for cereal disinfestations. *Mater. Res. Innov.* **2004**, *8*, 17–22. [CrossRef]
6. Oliveira, D.B.; Silva, E.J.; Santos, J.J.S.; Neto, O.M. Design of a microwave applicator for water sterilization using multiobjective optimization and phase control scheme. *IEEE Trans. Magn.* **2011**, *47*, 1242–1245. [CrossRef]
7. Lin, J.C.; Bernardi, P.; Pisa, S.; Cavagnaro, M.; Piuzzi, E. Antennas for medical therapy and diagnostics. In *Modern Antenna Handbook*; Balanis, C.A., Ed.; John Wiley & Sons Inc. Publication: Hoboken, NJ, USA, 2008; pp. 1377–1401.
8. Gupta, R.C.; Singh, S.P. Analysis of the SAR distributions in three-layered bio-media in direct contact with a water-loaded modified box-horn applicator. *IEEE Trans. Microw. Theory Tech.* **2005**, *53*, 2665–2671. [CrossRef]
9. Bucci, O.M.; Crocco, L.; Scapaticci, R.; Bellizzi, G. On the Design of Phased Arrays for Medical Applications. *Proc. IEEE Inst. Electr. Electron. Eng.* **2016**, *104*, 633–648. [CrossRef]
10. Curto, S.; McEvoy, P.; Bao, X.; Ammann, M.J. Compact patch antenna for electromagnetic interaction with human tissue at 434 MHz. *IEEE Trans. Antennas Propag.* **2009**, *57*, 2564–2571. [CrossRef]
11. Muntoni, G.; Fanti, A.; Montisci, G.; Muntoni, M. A blood perfusion model of a RMS tumor in a local hyperthermia multi-physic scenario: A preliminary study. *IEEE J. Electromagn. RF Microw. Med. Biol.* **2019**, *3*, 71–78. [CrossRef]
12. Singh, S.; Sahu, B.; Singh, S.P. Conformal microstrip slot antenna with an AMC reflector for hyperthermia. *J. Electromagn. Waves Appl.* **2016**, *30*, 1603–1619. [CrossRef]
13. Carlier, J.; Thomy, V.; Camart, J.C.; Dubois, L.; Pribetich, J. Modeling of planar applicators for microwave thermotherapy. *IEEE Trans. Microw. Theory Tech.* **2002**, *50*, 3036–3042. [CrossRef]
14. Attia, H.; Yousefi, L.; Ramahi, O.M. Analytical model for calculating the radiation field of microstrip antennas with artificial magnetic superstrates: Theory and experiment. *IEEE Trans. Antennas Propag.* **2001**, *59*, 1438–1445. [CrossRef]
15. Liu, Y.H.; Zhao, X.P. Investigation of anisotropic negative permeability medium cover for patch antenna. *IET Microw. Antennas Propag.* **2008**, *2*, 737–744. [CrossRef]
16. Attia, H.; Yousefi, L.; Bait-Suwailam, M.M.; Boybay, M.S.; Ramahi, O.M. Enhanced-gain microstrip antenna using engineered magnetic superstrates. *IEEE Antennas Wirel. Propag. Lett.* **2009**, *8*, 1198–1201. [CrossRef]
17. Jaffar, N.A.; Buniyamin, N.; Lias, K. An overview of available metamaterial-based antenna for non-invasive hyperthermia cancer treatment. *Indones. J. Electr. Eng. Comput. Sci.* **2019**, *14*, 697–705. [CrossRef]
18. Tao, Y.; Wang, G. Conformal hyperthermia of superficial tumor with left-handed metamaterial lens applicator. *IEEE. Trans. Biomed. Eng.* **2012**, *59*, 3525–3530. [CrossRef]
19. Gong, Y.; Wang, G. Superficial tumor hyperthermia with flat left-handed metamaterial lens. *Prog. Electromagn. Res. PIER* **2009**, *98*, 389–405. [CrossRef]

20. Vrba, D.; Vrba, J. Novel applicators for local microwave hyperthermia based on zeroth-order mode resonator metamaterial. *Int. J. Antennas Propag.* **2014**, *2014*, 631398. [CrossRef]
21. Vrba, D.; Rodrigues, D.B.; Vrba, J.; Stauffer, P.R. Metamaterial antenna arrays for improved uniformity of microwave hyperthermia treatments. *Prog. Electromagn. Res. PIER* **2016**, *156*, 1–12. [CrossRef]
22. Losito, O.; Portosi, V.; Venanzoni, G.; Bigelli, F.; Mencarelli, D.; Scalmati, P.; Renghini, C.; Carta, P.; Prudenzano, F. Feasibility investigation of SIW cavity-backed patch antenna array for Ku band applications. *Appl. Sci.* **2019**, *9*, 1271. [CrossRef]
23. Castellano, T.; Losito, O.; Mescia, L.; Chiapperino, M.A.; Venanzoni, G.; Mencarelli, D.; Angeloni, G.; Renghini, C.; Carta, P.; Prudenzano, F. Feasibility investigation of low cost substrate integrated waveguide (SIW) directional couplers. *Prog. Electromagn. Res. PIER* **2014**, *59*, 31–44. [CrossRef]
24. Mencarelli, D.; Morini, A.; Prudenzano, F.; Venanzoni, G.; Bigelli, F.; Losito, O.; Farina, M. Broadband single-layer slotted array antenna in SIW technology. *IEEE Antennas Wirel. Propag. Lett.* **2016**, *15*, 263–265. [CrossRef]
25. Chiapperino, M.A.; Losito, O.; Castellano, T.; Venanzoni, G.; Mescia, L.; Angeloni, G.; Renghini, C.; Carta, P.; Potenza, P.; Prudenzano, F. Dual-Band substrate integrated waveguide resonator based on sierpinski carpet. *Prog. Electromagn. Res. PIER* **2015**, *57*, 1–12. [CrossRef]
26. Venanzoni, G.; Mencarelli, D.; Morini, A.; Farina, M.; Losito, O.; Prudenzano, F. Compact substrate integrated waveguide six-port directional coupler for X-band applications. *Microw. Opt. Technol. Lett.* **2015**, *57*, 2589–2592. [CrossRef]
27. Venanzoni, G.; Mencarelli, D.; Morini, A.; Farina, M.; Losito, O.; Prudenzano, F. Compact double-layer substrate integrated waveguide magic Tee for X-band applications. *Microw. Opt. Technol. Lett.* **2016**, *58*, 932–936. [CrossRef]
28. Venanzoni, G.; Mencarelli, D.; Morini, A.; Farina, M.; Prudenzano, F. Review of substrate integrated waveguide circuits for beam-forming networks working in X-band. *Appl. Sci.* **2019**, *9*, 3. [CrossRef]
29. Balanis, C.A. *Antenna Theory Analisys and Design*, 4th ed.; John Wiley & Sons, Inc.: Hoboken, NJ, USA, 2016.
30. Zhang, X.; Robinson, M.; Flintoft, I.D.; Dawson, J.F.; Parker, S. Morphological Study on Human Body Absorption Cross Section in a Reverberation Chamber From 1 GHz to 16 GHz. *IEEE Trans. Electromagn. Compat.* **2020**, *62*, 330–337. [CrossRef]
31. Pendry, J.B.; Holden, A.J.; Robbins, D.J.; Stewart, W.J. Magnetism from conductors and enhanced Nonlinear phenomena. *IEEE Trans. Microw. Theory Tech.* **1999**, *47*, 2075–2084. [CrossRef]
32. Caloz, C.; Itoh, T. *Electromagnetic Metamaterials: Transmission Line Theory and Microwave Applications*; Wiley & IEEE Press: Hoboken, NJ, USA, 2006.
33. Maslovski, S.; Ikonen, P.; Kolmakov, I.; Tretyakov, S. Artificial magnetic material based on the new magnetic particle: Metasolenoid. *Prog. Electromagn. Res. PIER* **2005**, *54*, 61–81. [CrossRef]
34. Collin, R.E. *Foundation for Microwave Engineering*, 2nd ed.; John Wiley & Sons, Inc.: Hoboken, NJ, USA, 2001.
35. Andreuccetti, D.; Fossi, R.; Petrucci, C. *An Internet Resource for the Calculation of the Dielectric Properties of Body Tissues in the Frequency Range 10 Hz–100 GHz*; IFAC-CNR: Florence, Italy, 1997; Available online: http://niremf.ifac.cnr.it/tissprop (accessed on 4 September 2020).
36. Velázquez-Ahumada, M.C.; Freire, M.J.; Marqués, R. Metamaterial focusing device for microwave hyperthermia. *Microw. Opt. Technol. Lett.* **2011**, *53*, 2868–2872. [CrossRef]
37. Leggio, L.; de Varona, O.; Dadrasnia, E. A comparison between different schemes of microwave cancer hyperthermia treatment by means of left-handed metamaterial lenses. *Prog. Electromagn. Res. PIER* **2015**, *150*, 73–87. [CrossRef]
38. Lias, K.; Buniyamin, N.; Zulkarnaen, M. Simulation study of an EBG-M applicator towards non-invasive breast hyperthermia cancer procedure. *J. Teknol.* **2016**, *78*, 75–81. [CrossRef]
39. Tao, Y.; Yang, E.; Wang, G. Left-handed metamaterial lens applicator with build-in cooling feature for superficial tumor hyperthermia. *Appl. Comput. Electromagn. Soc. J.* **2017**, *32*, 1029–1034.